Biophysical Journal, Volume *121*

Supplemental information

An internal docking site stabilizes substrate binding to γ-secretase: Analysis by molecular dynamics simulations

Shu-Yu Chen and Martin Zacharias

Supporting Information:
An internal docking site stabilizes substrate binding to γ-secretase: Analysis by Molecular Dynamics Simulations

Shu-Yu Chen[1], Martin Zacharias[1,*]

[1]Physics Department and Center of Functional Protein Assemblies, Technical University of Munich, 85748 Garching, Germany

(A)

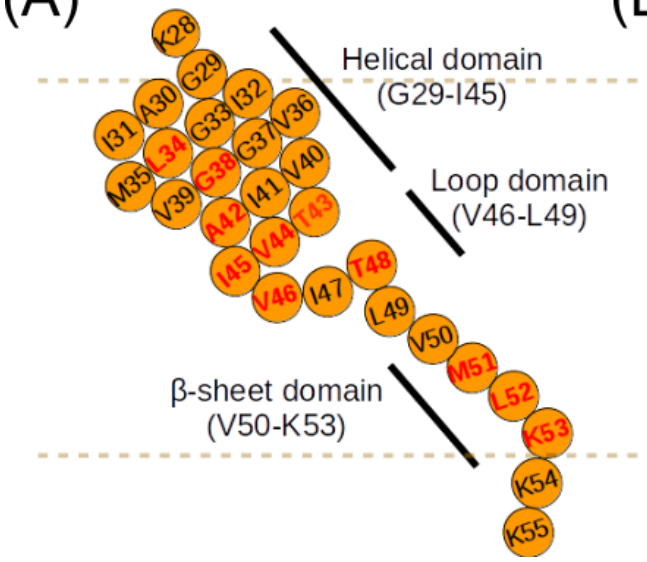

(B)

Residue	Domain	FAD Mutation
L34	Helical	L34V
G38	Helical	G38S
A42	Helical	A42T,A42V
T43	Helical	T43A,T43I
V44	Helical	V44A,V44M
I45	Helical	I45F,I45M,I45T,I45V
V46	Loop	V46F,V46G,V46I,V46L
T48	Loop	T48P,T48N
M51	β-sheet	M51K
L52	β-sheet	L52P
K53	β-sheet	K53N

Figure S1: FAD mutations on the transmembrane domain of APP according to https://www.alzforum.org/ (A) Illustration of the position of FAD mutant points (red) mapping into helical, loop and β-sheet domains based on the secondary structure resolved in the C83-bound Cryo-EM structure. (PDBID 6IYC) **(B)** Table of FAD mutations reported on https://www.alzforum.org**.**

.

(A)

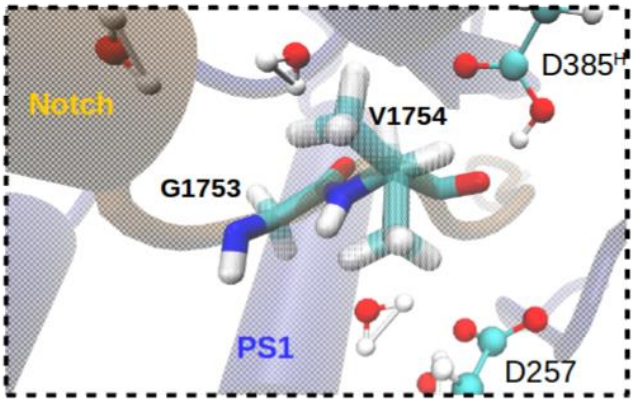

(B)

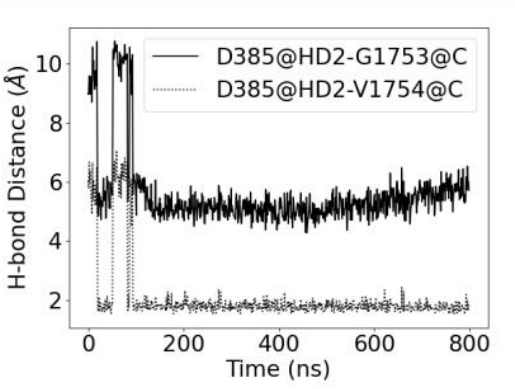

Figure S2: Simulation of the Notch-bound γ-secretase complex with D385-protonated PS1 starting with the structure derived from PDBID 6IDF. (**A**) Schematic view of at the catalytic center (snapshot). Waters within 5Å from V1754 are drawn in the CPK representation. Note that the bond between G1753 and V1754 is the correct S3 site to be cleaved (1). (**B**) Distances between the protonated D385 and the carbonyl group of G1753 (solid) of V1754 (dotted) of Notch1.

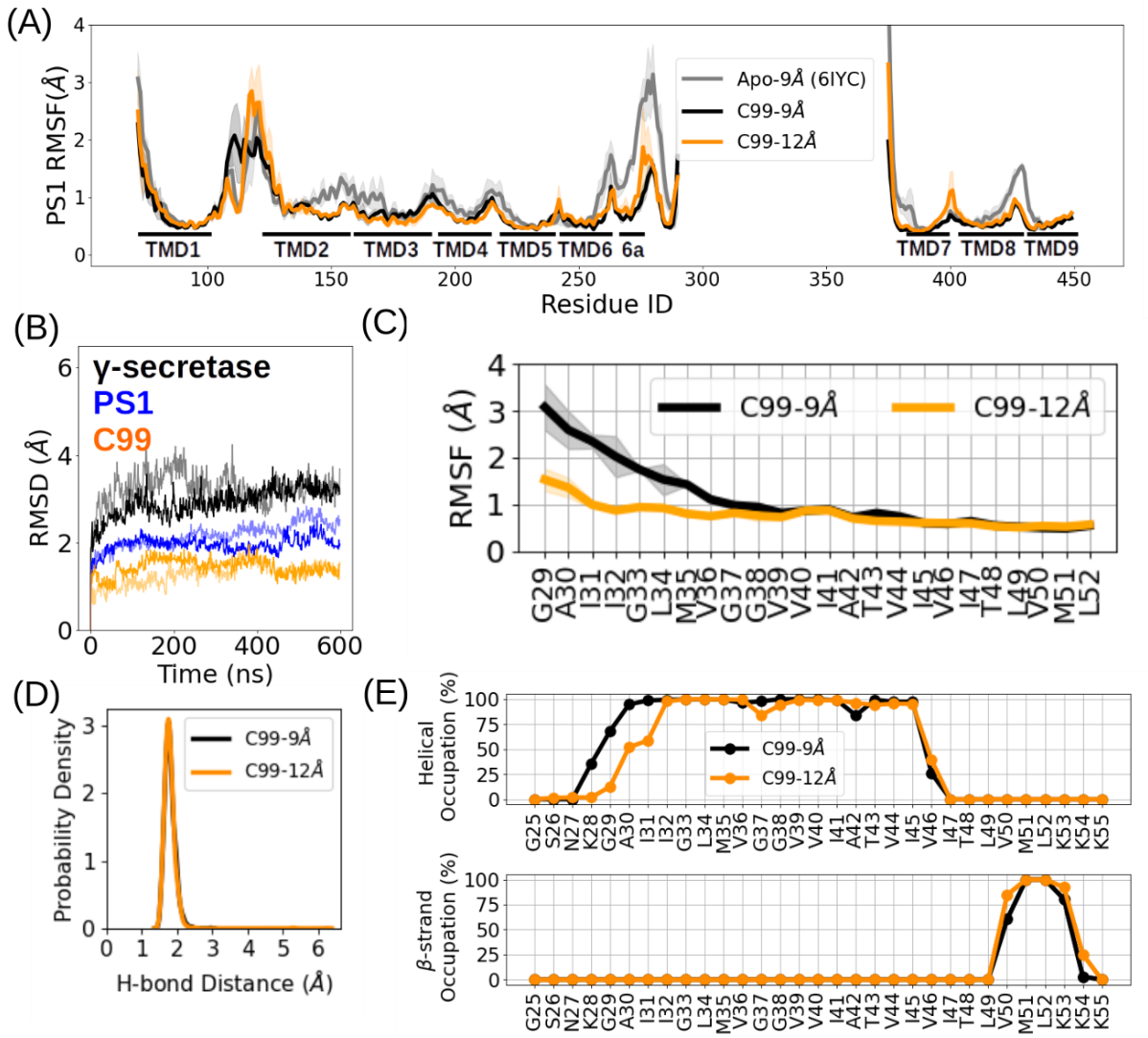

Figure S3: Comparison of C99-bound complex simulations with a non-bonded cutoff distance 9 Å (black) or 12 Å (orange). (A) RMSF of PS1. **(B)** RMSD of γ-secretase (black), the catalytic unit presenilin-1 (PS1, blue) and substrate (orange) for the 12Å cutoff (two independent simulations indicated by solid and transparent lines). **(C)** RMSF of C99 (trajectory with highest difference selected). **(D)** Catalytic hydrogen bond frequency. **(E)** Secondary structure analysis averaged over 2 independent trajectories. Note that the higher RMSF at the N-terminal half of C99 in the 9Å cutoff simulation (shown in C) was only observed in one simulation. In all other simulations, the substrates showed an RMSF lower than 2 Å at the N-terminal half of the substrate, including the most unstable substrate Aβ40$_{γ37}$ **(**see **Figure S22A).**

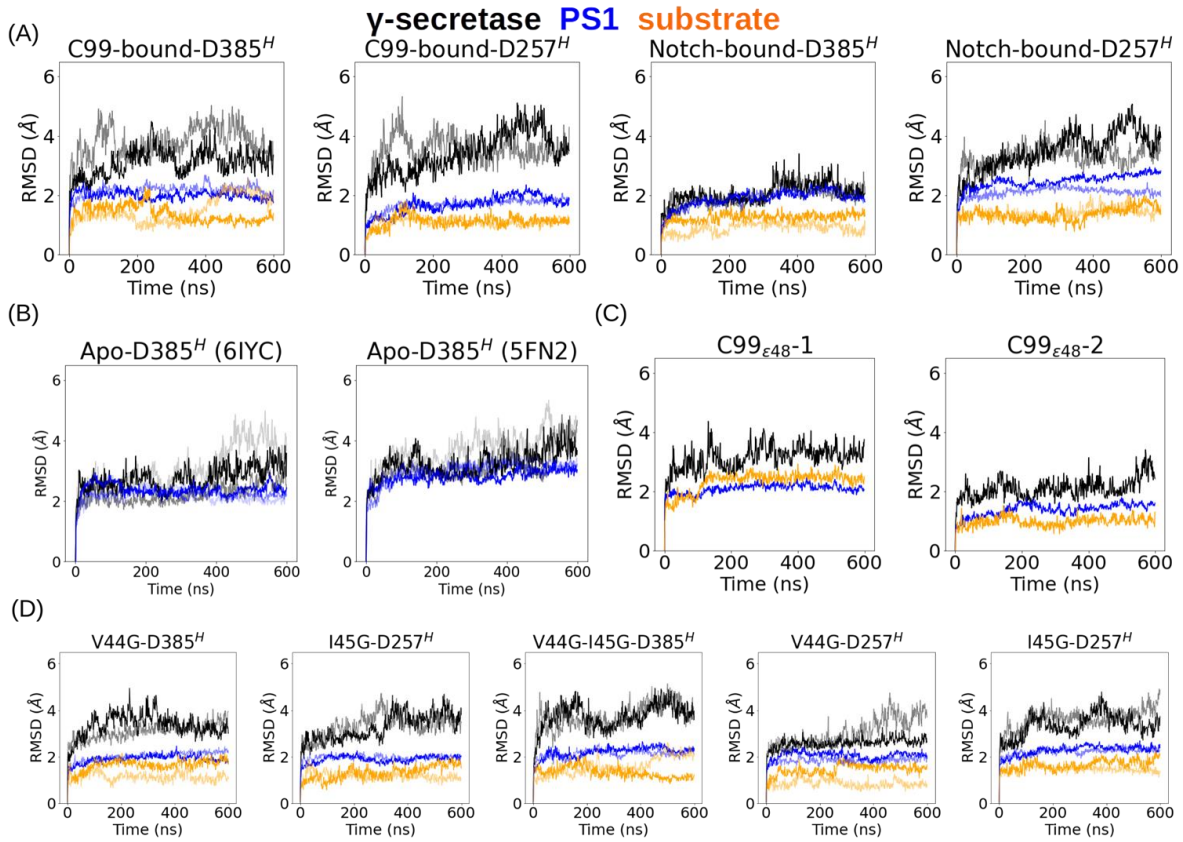

Figure S4: RMSD of γ-secretase (black), the catalytic unit presenilin-1 (PS1, blue) and substrate (orange) vs. time in apo- and bound-states. (A) C99 or Notch-bound states. **(B)** The apo-form with PDBID 6IYC or 5FN2 as the initial and reference structure. **(C)** RMSD vs. time during the ε48 binding pose simulations. **(D)** RMSD vs. time during simulation of C99 mutants in bound states. The results for the first replica of each system is shown as the solid line and for the second replica as transparent line. The third replica of the apo-state simulation is shown as an even lighter transparent line. The protonation states of PS1 residues $D385^{H}$ and $D257^{H}$ are indicated.

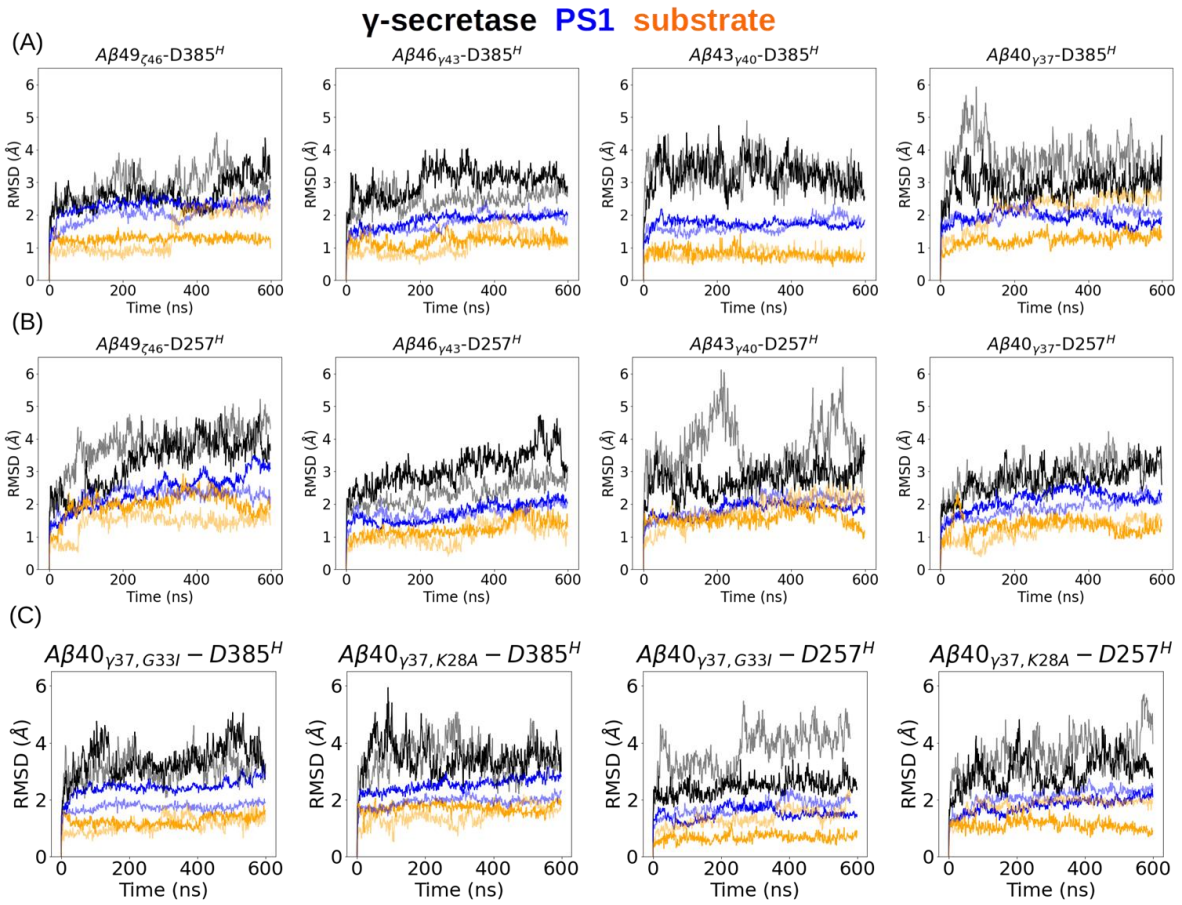

Figure S5: RMSD of γ-secretase (black), the catalytic unit presenilin-1 (PS1, blue) and substrate (orange) vs. time in complex with various Aβ peptides. (A) RMSD vs. time for simulations with different Aβ peptides bound to the $D385^H$ γ-secretase, **(B)** RMSD vs. time for simulations with different Aβ peptides bound to the $D257^H$ γ-secretase, and **(C)** RMSD vs. time for simulations with different Aβ40 mutants bound to either $D385^H$ or $D257^H$ γ-secretase. The results for the first replica of each system is shown as the solid line and for the second replica as transparent line.

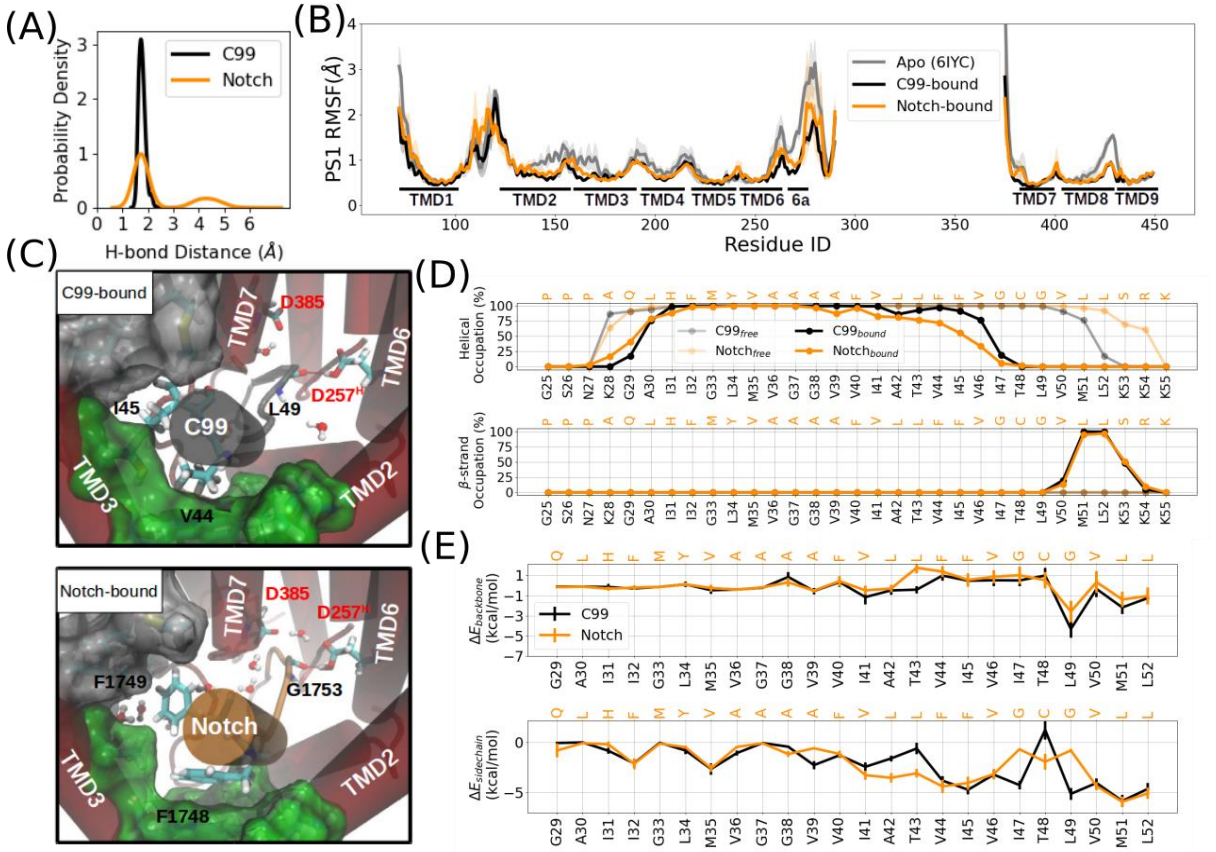

Figure S6: Simulations of the Notch, C99 and γ-secretase in the bound and apo (free) forms with D257-protonated PS1. (A) Probability density distribution of the catalytic hydrogen bond distance. **(B)** Residue-wise root-mean-square fluctuation (RMSF) of the γ-secretase catalytic subunit PS1. Apo-form γ-secretase structures are derived from PDB entry 6IYC. **(C)** Top-view at the PS1 internal docking site in the C99-bound (top) and Notch-bound (bottom) γ-secretase complexes. PS1 is shown in the blue cartoon representation and substrate in grey and Notch in orange. The subpocket formed by TMD2-TMD3 is shown as green surface, and the subpocket formed by TMD3-TMD5 and TMD7 is shown as white surface. Residues that form part of these two pockets are listed in **Table 2** in the main text. Water molecules are shown in the vdw+bond representation. V44, I45 and the backbone of L49 of C99 and F1748, F1749 and the backbone of G1753 of Notch are shown in the licorice representation. The catalytic hydrogen bond is shown as the red dashed line between the substrate scissile bond and the protonated aspartic acid. **(D)** Secondary structure analysis of C99 (black) and Notch (orange) in γ-secretase bound form (solid line) and free form (transparent line). Helical (top) and β-sheet (bottom) occupations are calculated by averaging over two replicas. **(E)** Residue-wise binding energy decomposition between γ-secretase and C99 (black) or Notch (blue). Backbone (top) and sidechain (bottom) contributions are averaged over two replicas.

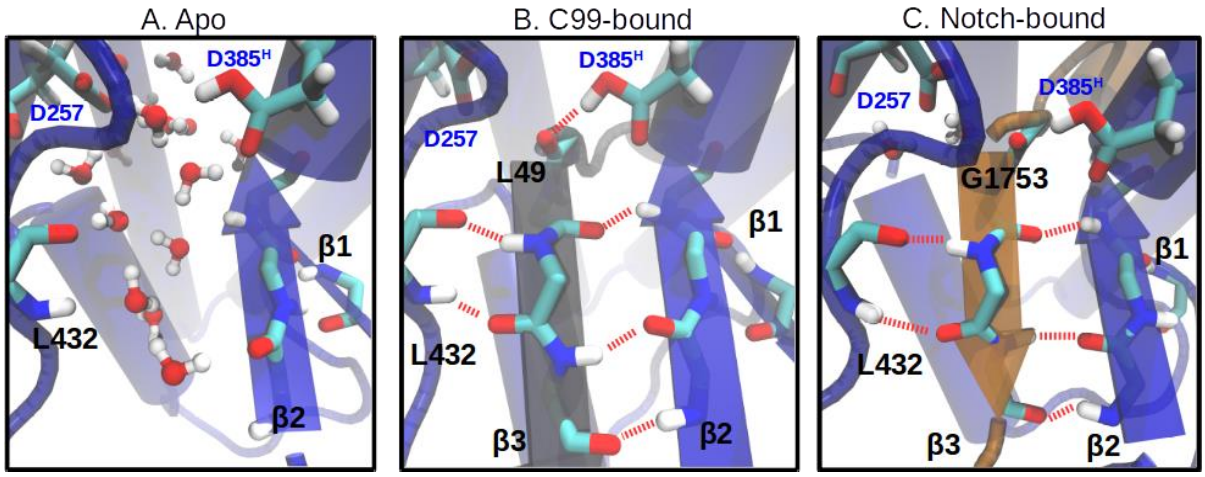

Figure S7: Schematic views of the post-cleavage site β-sheet cluster in the Apo (A), C99-bound (B), and Notch-bound (C) γ-secretase complexes with D385-protonated PS1. The corresponding residues of each β-strand component are listed in Figure 1A of the main text.

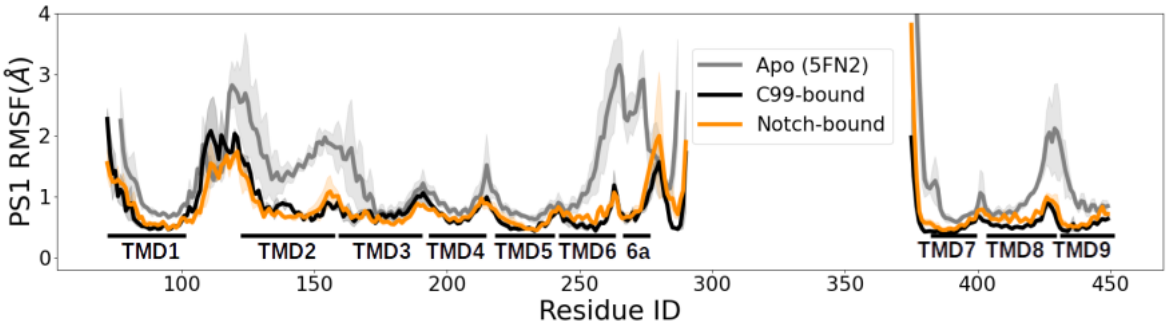

Figure S8: Comparison of PS1 RMSF between the Apo-state starting from the 5FN2 structure (grey), the C99-bound (black), and the Notch-bound (orange) states with D385-protonated PS1.

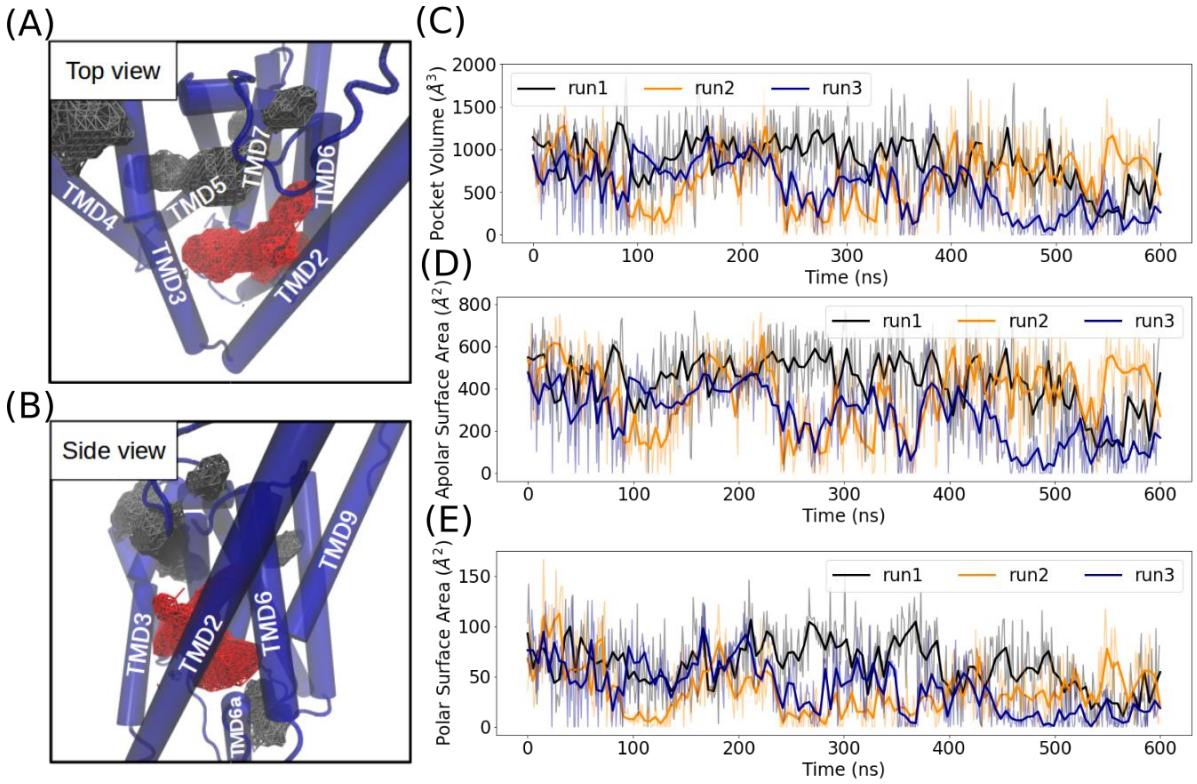

Figure S9: Pocket detection analysis on the γ-secretase Apo-state simulation with PDBID 6IYC as initial structure. (A) The top view and **(B)** side view of the Apo-state γ-secretase and pockets detected inside γ-secretase. The proposed internal docking site is highlighted in red. **(C)** Time evolution of the internal docking site pocket volume. **(D)** Time evolution of the internal docking site pocket apolar surface area. **(E)** Time evolution of the internal docking site pocket polar surface area. Three replicas of Apo-state simulations are shown in black, orange, and dark-blue, respectively. Solid lines show the averaged values over every 5ns from the transparent lines with 1ns time interval.

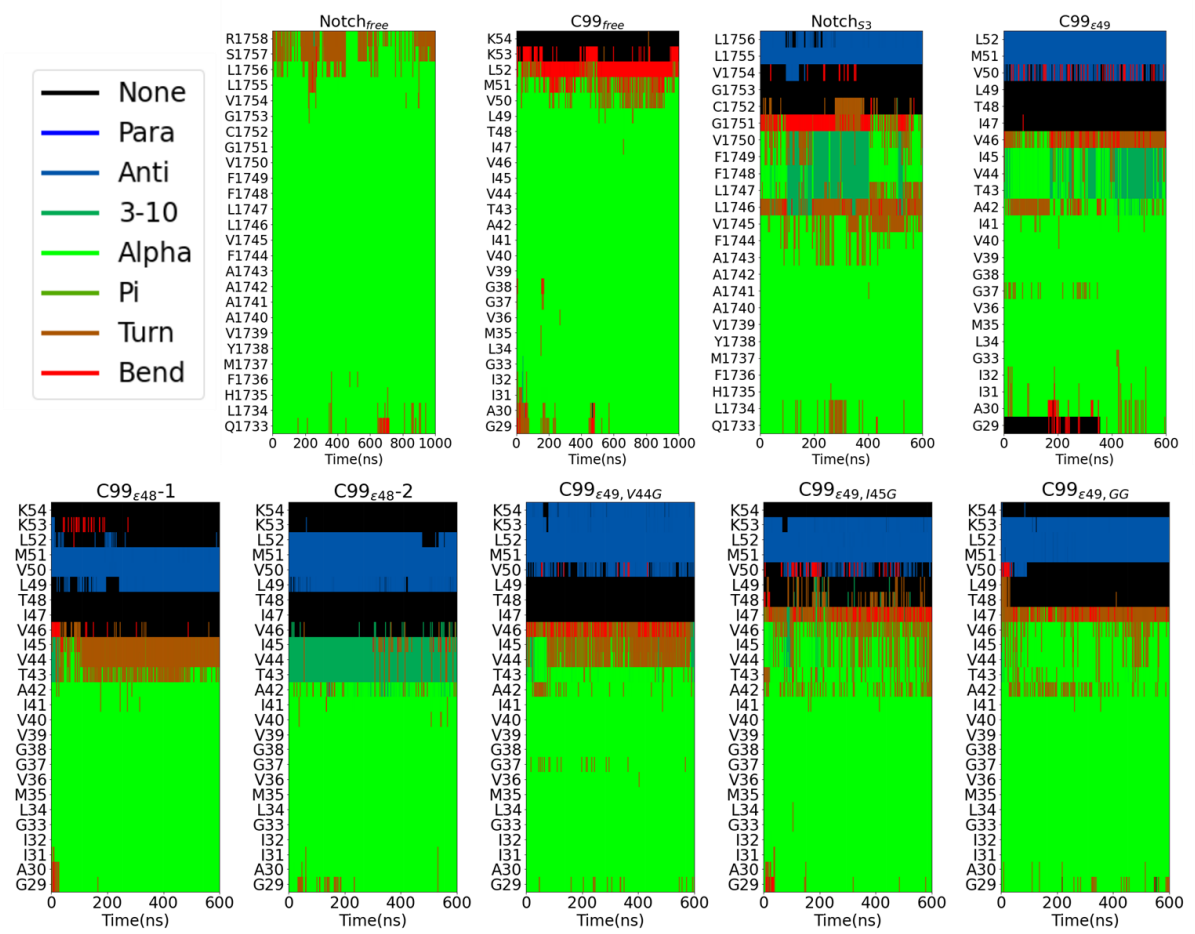

Figure S10: Time evolution of secondary structure of the substrates during simulations. (From left to right) Top: Free state Notch, free state C99, bound state Notch, bound state C99. Bottom, variants: C99$_{\varepsilon 48}$-1, C99$_{\varepsilon 48}$-2, C99$_{V44G}$, C99$_{I45G}$, C99$_{GG}$.

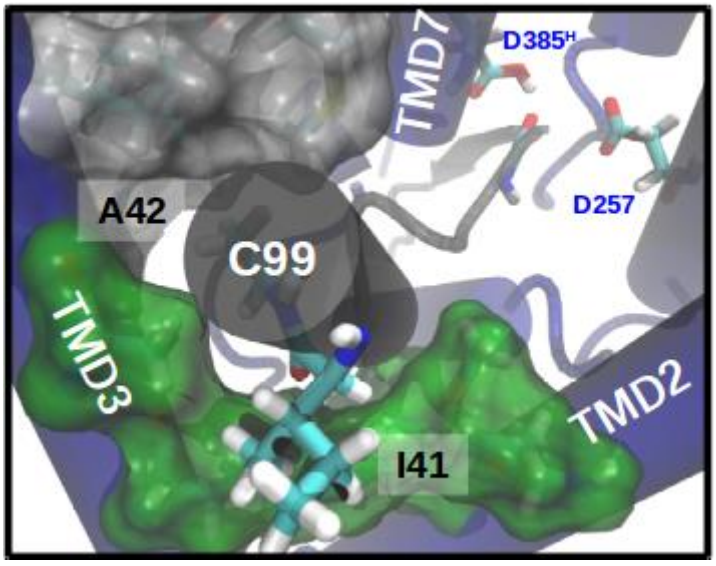

Figure S11: Top view at the PS1 internal docking site at the C99$_{\varepsilon 49}$ binding pose with A42 and I41 well aligned to the PS1 internal docking site.

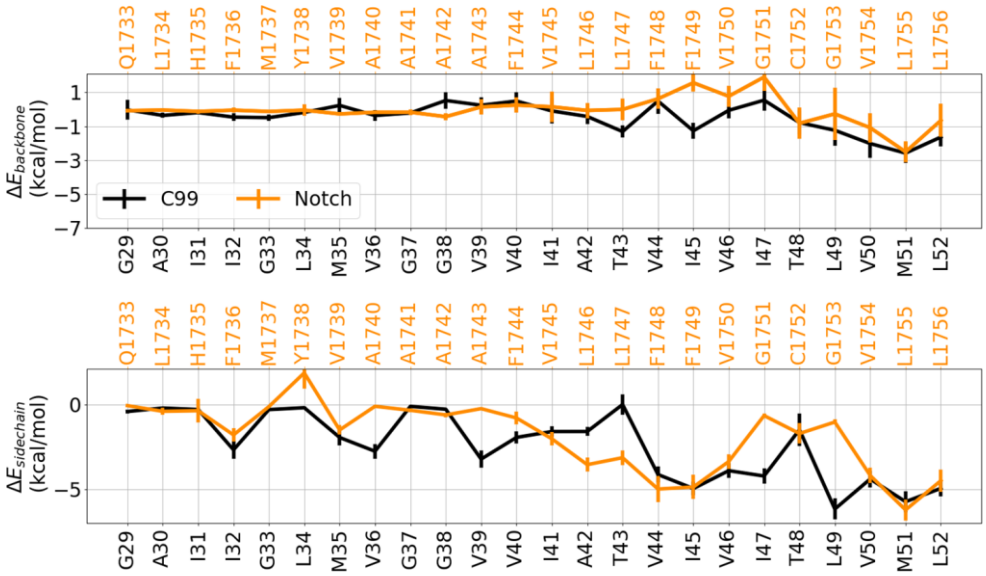

Figure S12: Residue-wise binding energy decomposition between γ-secretase and substrate C99 (black) or Notch (orange). Backbone (top) and sidechain (bottom) contributions are averaged over the trajectories of two MD simulations.

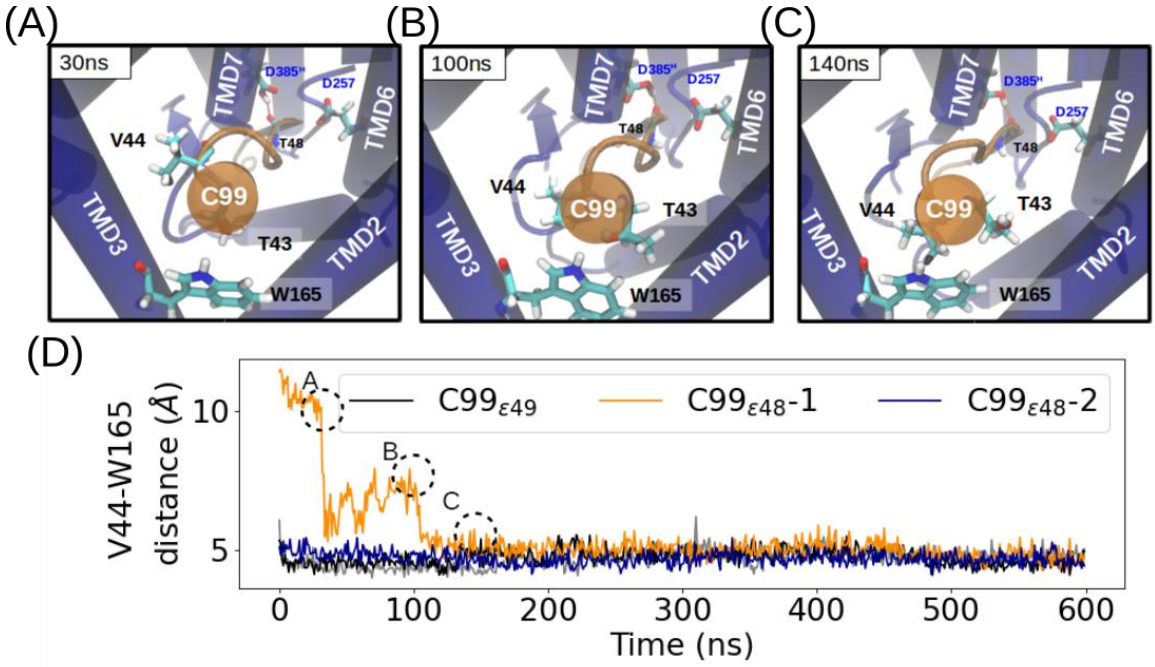

Figure S13: Rotation of the C99 helical domain observed in the C99$_{ε48}$-1 simulation. Snapshots of the rotational movement at **(A)** 30ns, **(B)** 100ns, and **(C)** 140ns. PS1 is shown in blue and C99 is shown in orange. **(D)** The center-of-mass (COM)-COM distance between V44 of C99 and W165 of PS1 during each 600ns simulation of C99$_{ε49}$ (black and gray), C99$_{ε48}$-1 (orange), and C99$_{ε48}$-2 (darkblue) binding to γ-secretase. The representative time frames of C99$_{ε48}$-1 are encircled and shown in (A)-(C). The animated process is shown in **Video S1**.

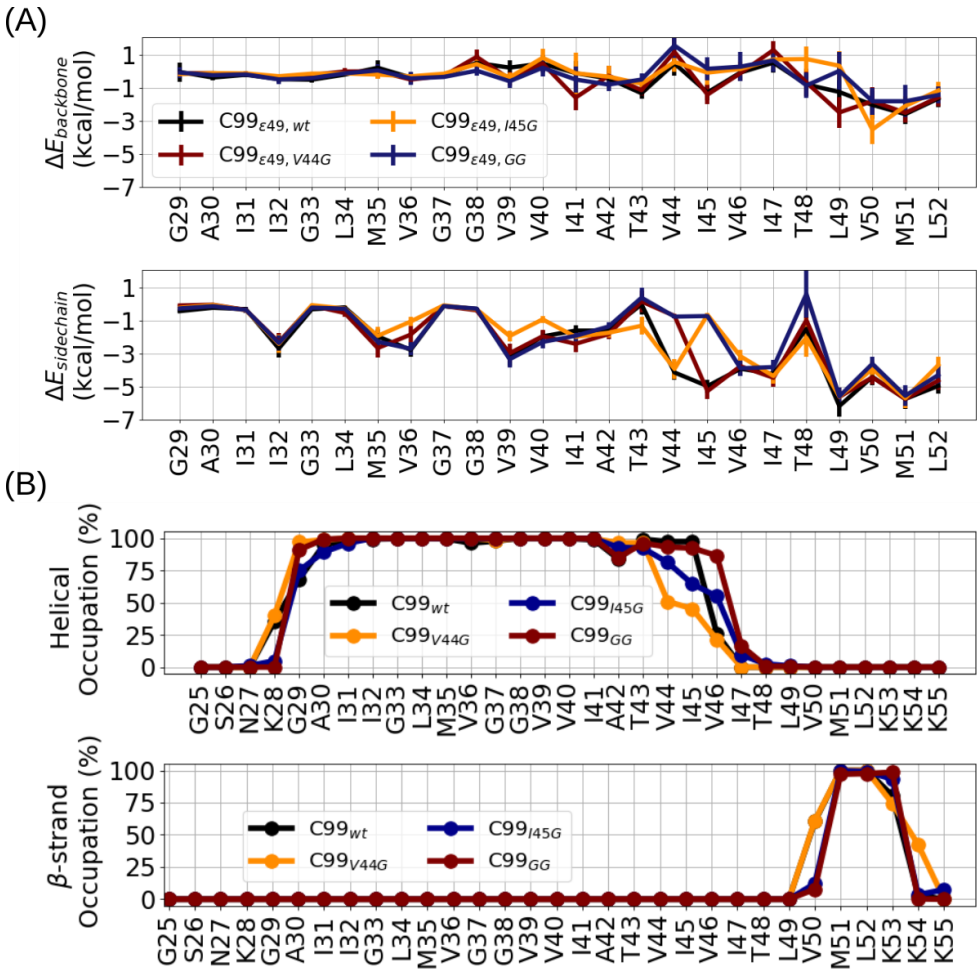

Figure S14: Analysis of the residue-wise binding energy decomposition (A) and secondary structures (B) in the V44G (orange), I45G (dark blue), and V44G+I45G (GG, brown) mutated complexes in comparison to the wild type C99 (black) with D385-protonated PS1.

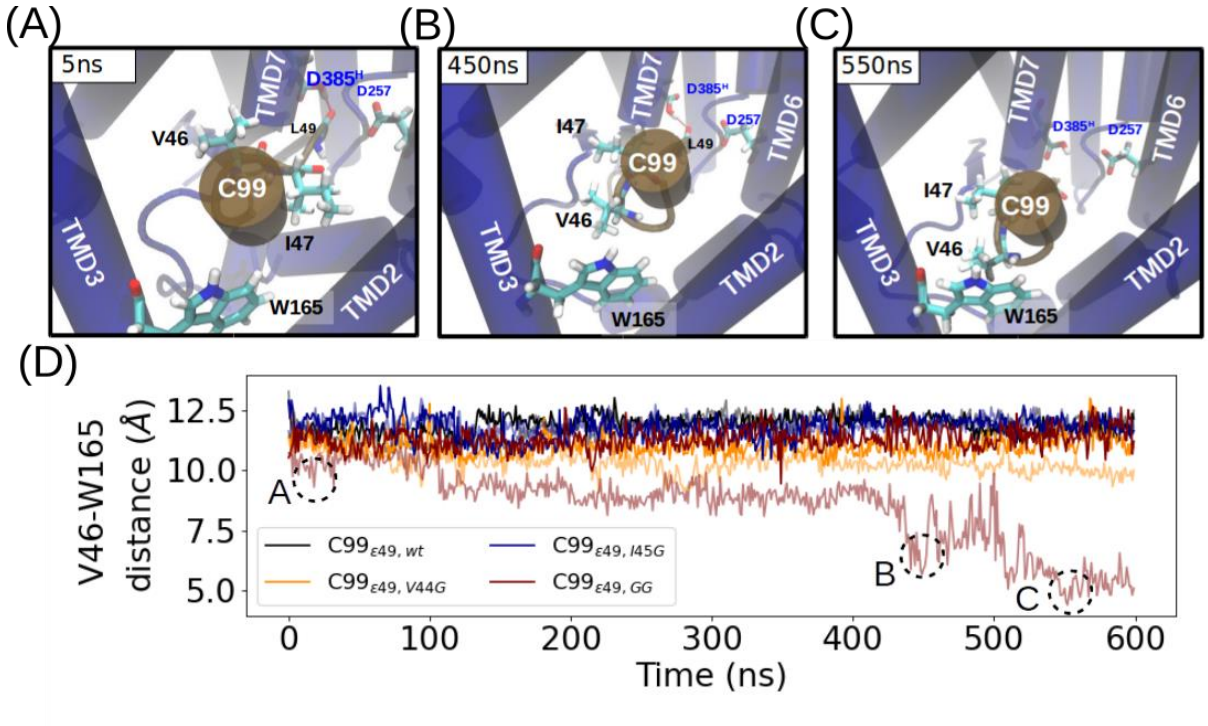

Figure S15: Rotation of the C99 helical domain observed in one of the $C99_{GG}$ simulation. Snapshots of the rotational movement at **(A) 5**ns, **(B)** 450ns, and **(C)** 550ns. PS1 is shown in blue and $C99_{GG}$ is shown in brown. **(D)** The center-of-mass (COM)-COM distance between V46 of C99 and W165 of PS1 during each 600ns simulation of $C99_{\varepsilon 49}$ (black and gray), $C99_{\varepsilon 48}$-1 (orange), and $C99_{\varepsilon 48}$-2 (dark-blue) binding to γ-secretase. The representative time frames of $C99_{GG}$ are encircled and shown in (A)-(C).

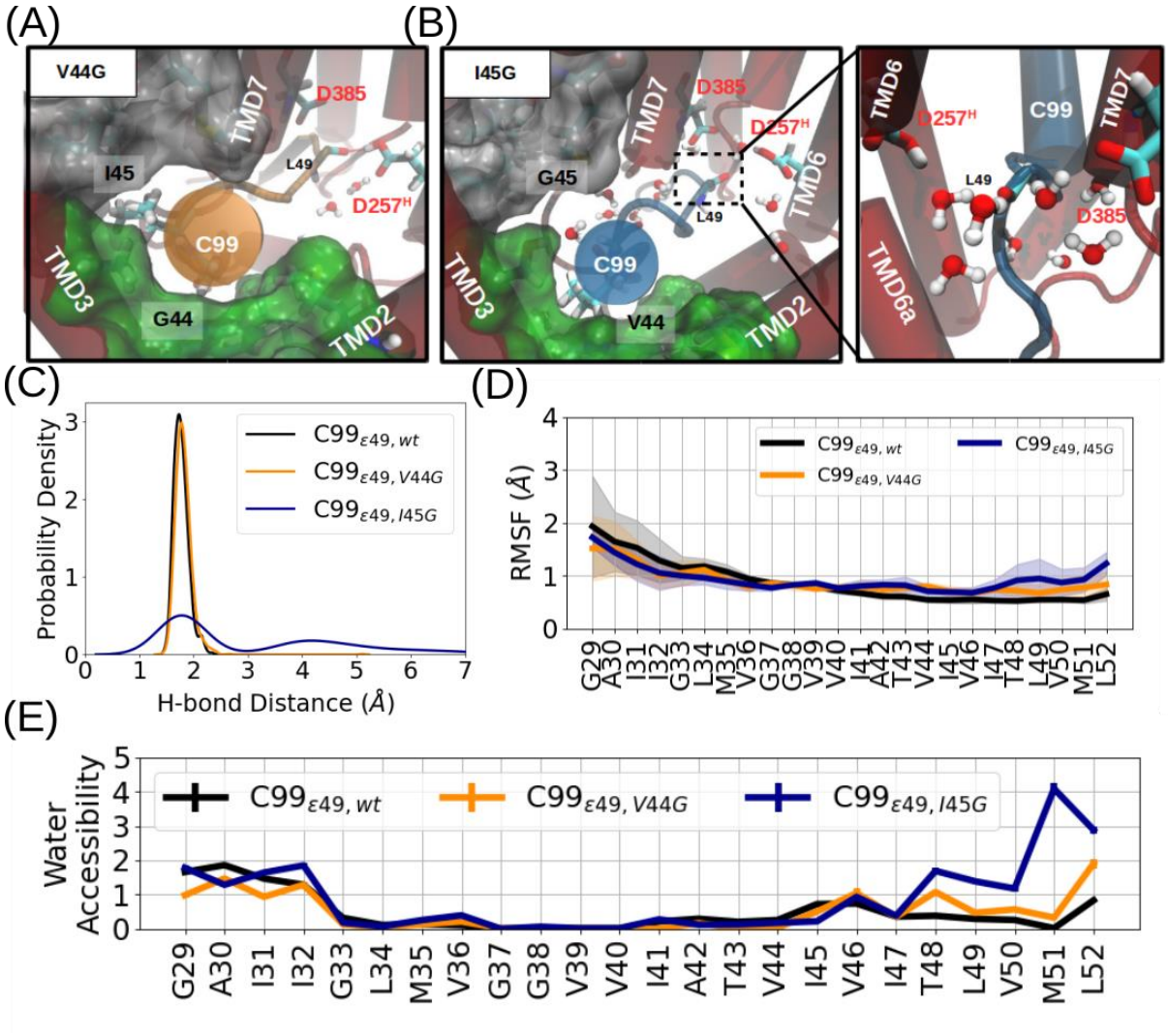

Figure S16: Glycine mutations at the internal docking site disturb the E-S interaction with D257-protonated PS1. (A) Top-view at the PS1 internal docking site of $C99_{V44G}$ bound γ-secretase complex. **(B)** Top-view at the PS1 internal docking site $C99_{I45G}$ bound γ-secretase complex with a zoom-in view shows the dissociated β-strand. Atomic representations are similar as described in **Figure S6C**. **(C)** Probability density of the catalytic hydrogen bond distance, **(D)** RMSF of the substrate TMD, and **(E)** secondary structure analysis. of $C99_{wt}$ (black), $C99_{V44G}$ (orange), and $C99_{I45G}$ (dark blue) in γ-secretase bound form.

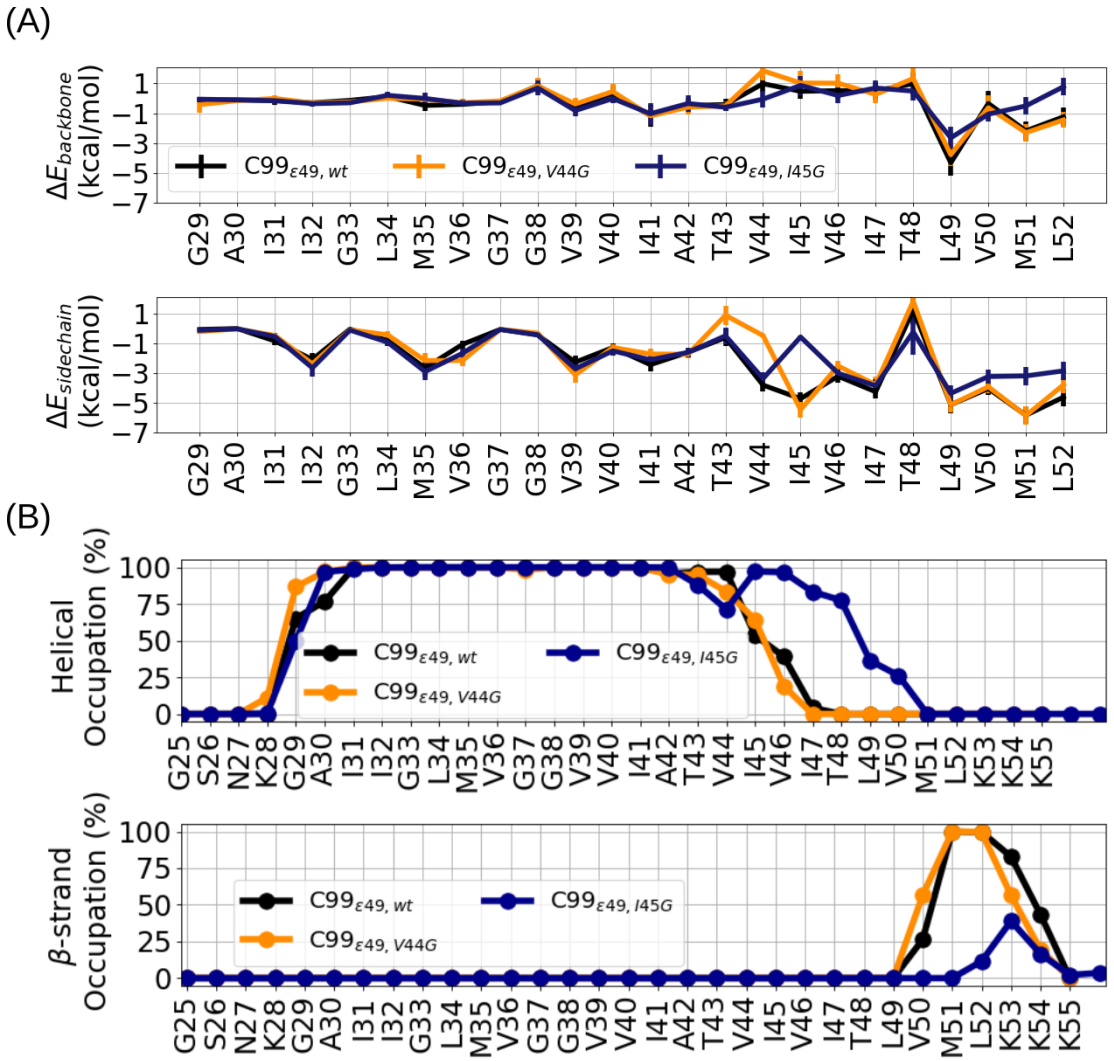

Figure S17: Analysis of the (A) residue-wise binding energy decomposition and (B) secondary structures in the V44G (orange) and I45G (dark blue) mutated complexes in comparison to the wildtype C99 (black) with D257-protonated PS1.

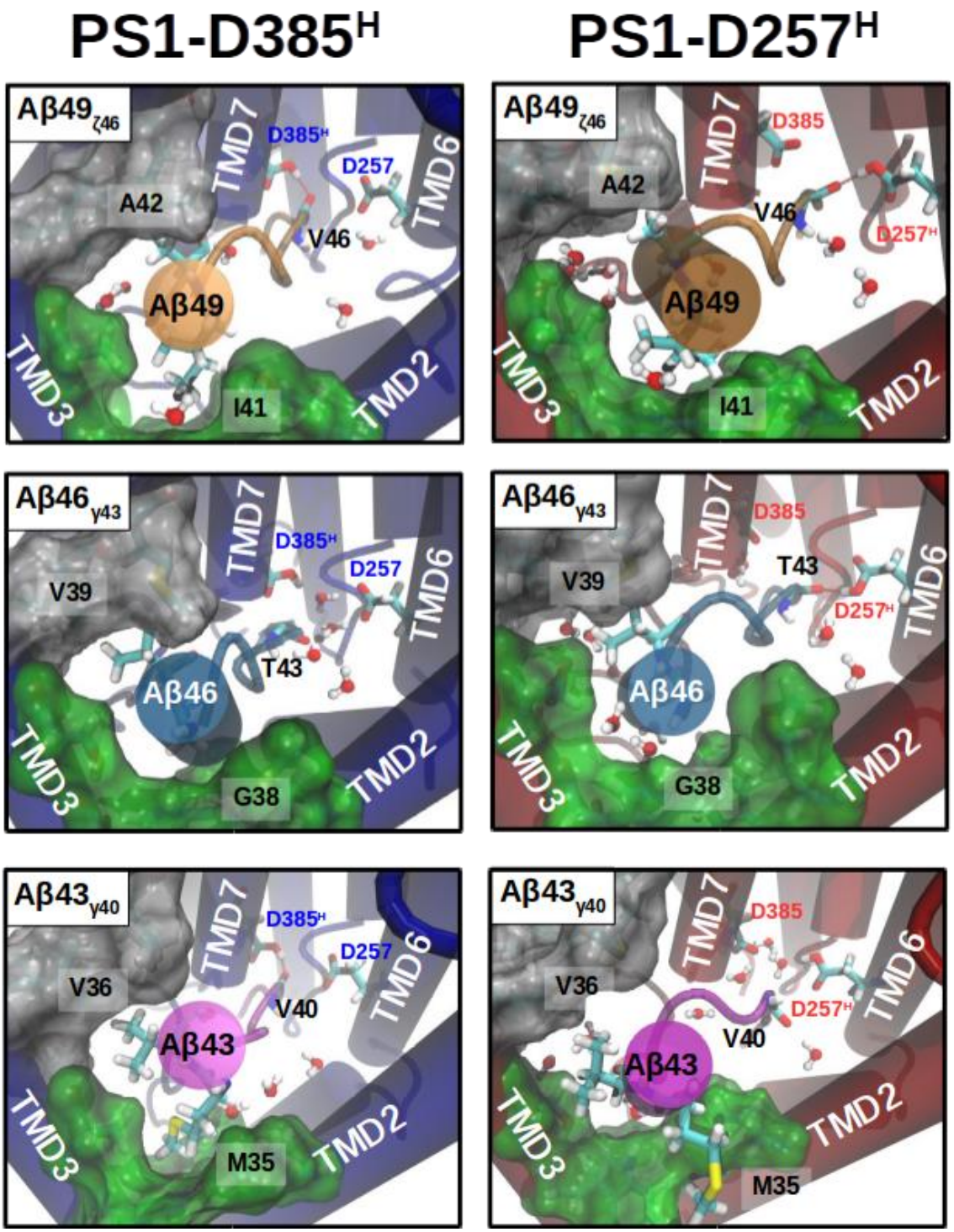

Figure S18: Top view of different Aβ peptides binding to the PS1 internal docking site with (left) D385-protonated or (right) D257-protonated. From top to bottom: $Aβ49_{ζ46}$, $Aβ46_{γ43}$, $Aβ43_{γ40}$. Atomic representations are similar as described in Figure S6C.

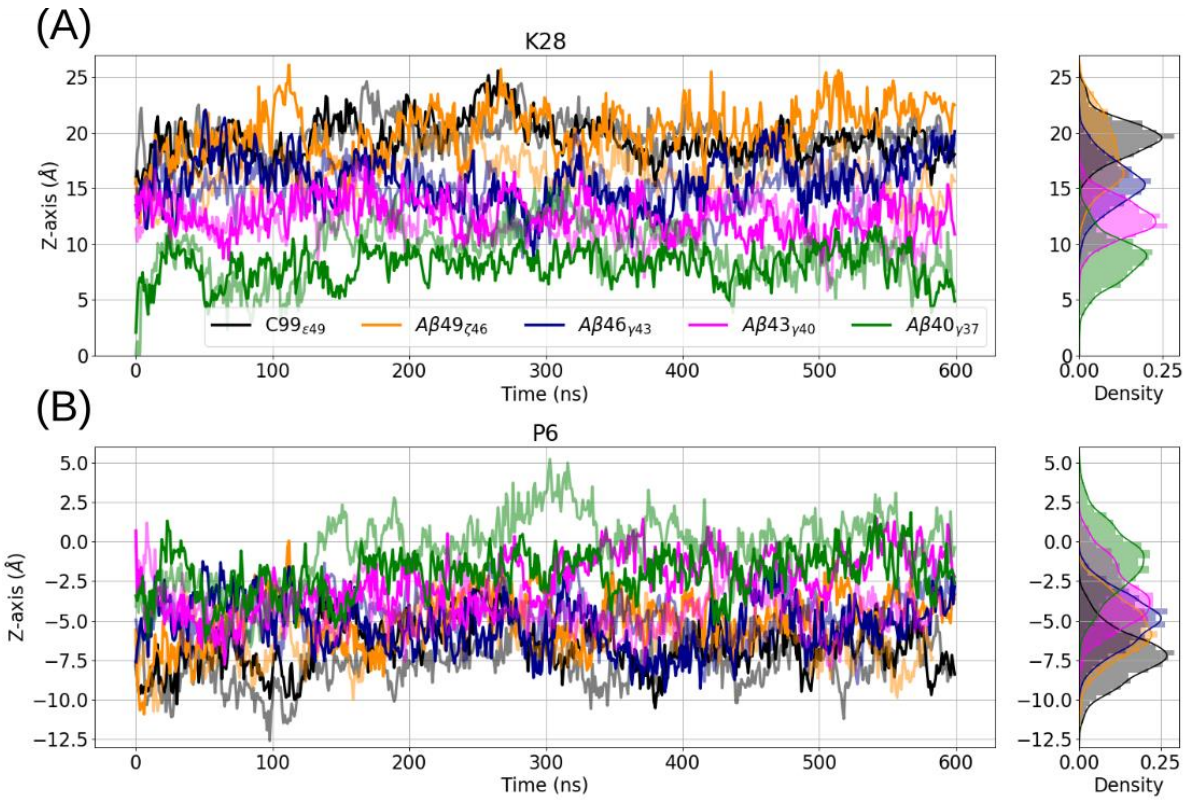

Figure S19: Z-axis position of substrate (A) K28 and (B) P6 in complex with γ-secretase with D385-protonated vs. simulation time. Two replicas are represented by solid and transparent lines in the same color. The averaged phosphate groups are located at z=18Å plane (see Figure 5D in the main text).

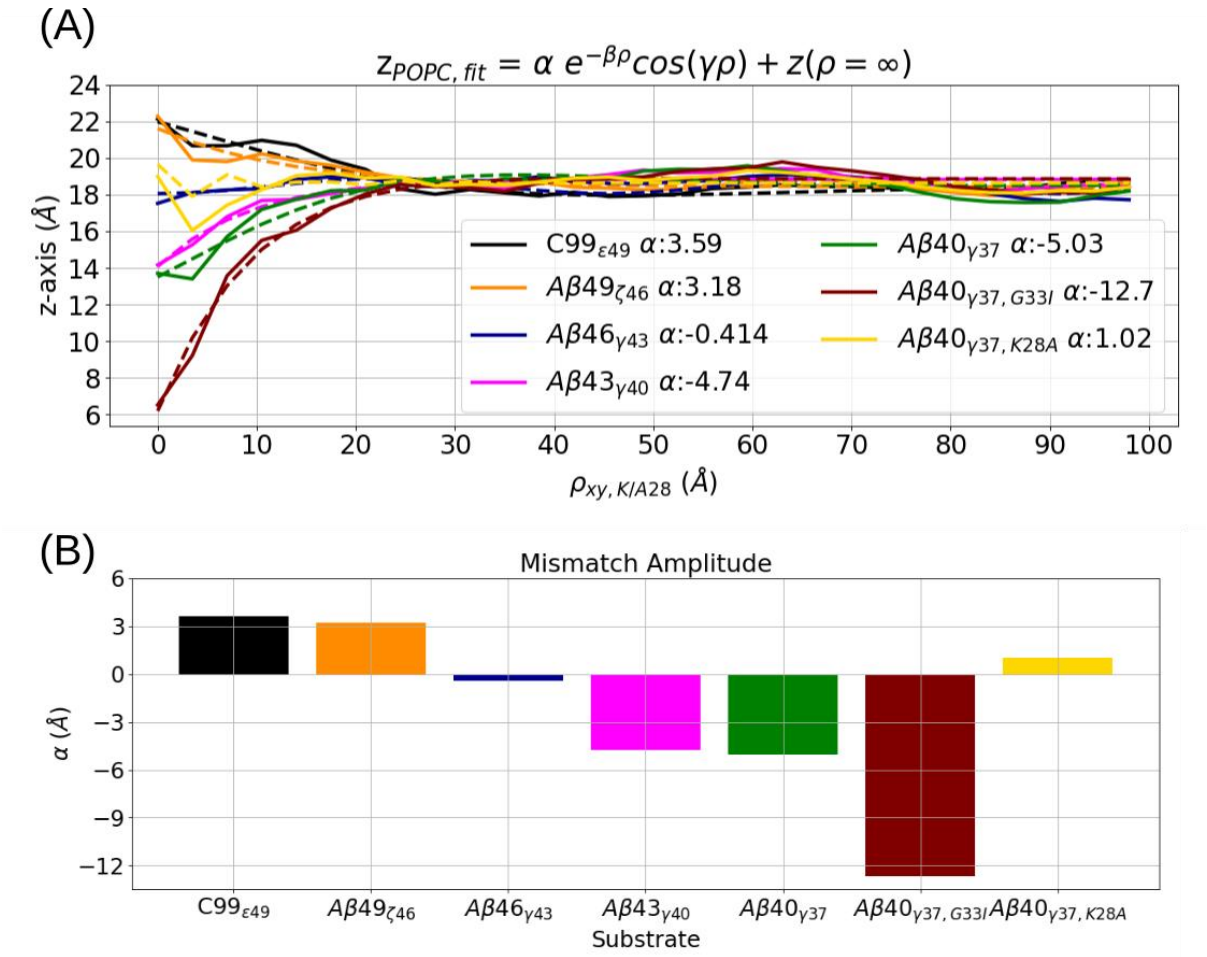

Figure S20: Fitting of the membrane thickness distributed alone the radial distance on the xy plane from K/A28 of substrates with D385-protonated PS1. **(A)** Fitting the hydrophobic mismatch profile with hydrophobic mismatch amplitude α, radial decaying rate β, and harmonic oscillation γ. **(B)** Comparison of the hydrophobic mismatch amplitude α calculated from **(A)** in different Aβ-bound γ-secretase structures.

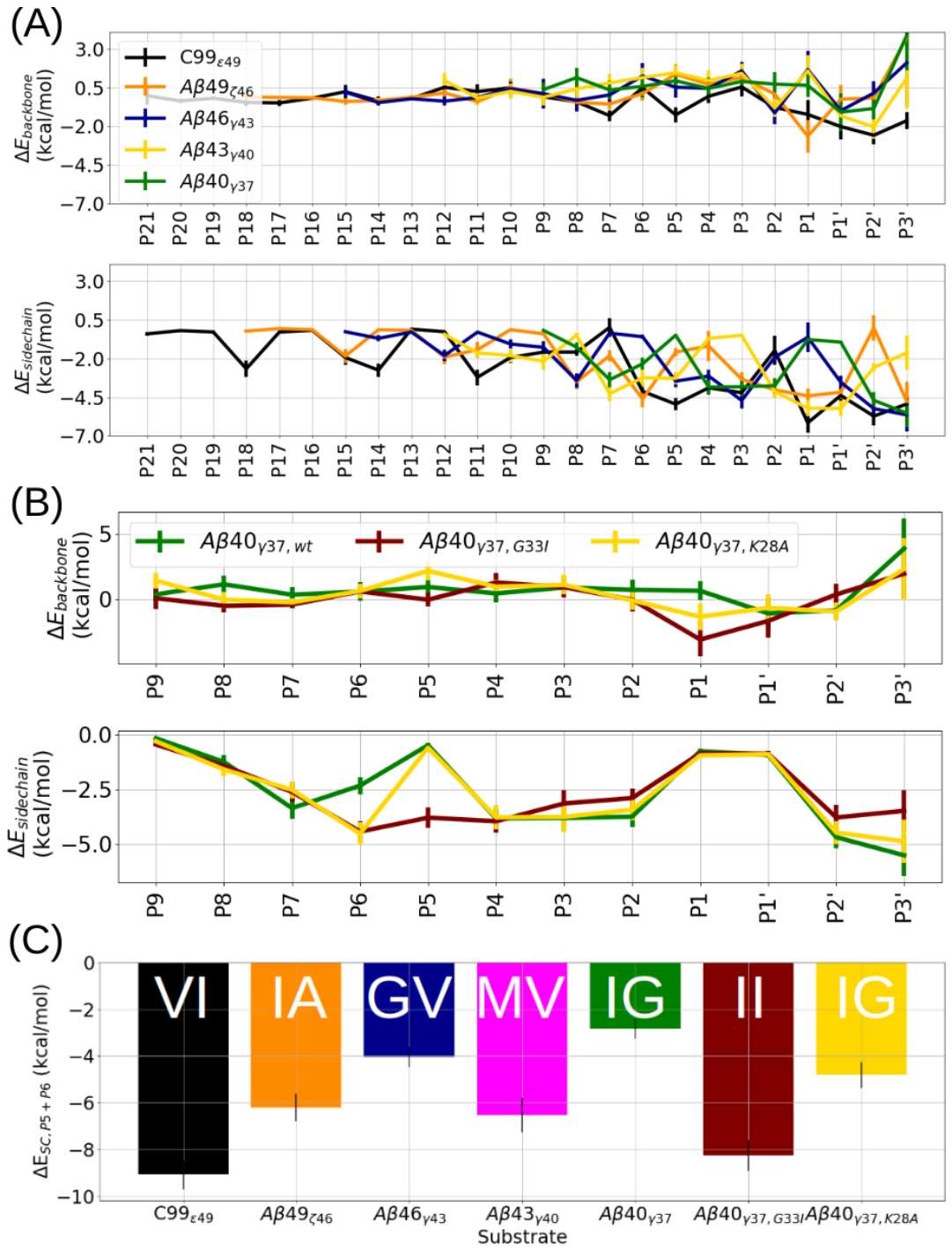

Figure S21: Calculated MMGBSA interaction energy between different Aβ substrates and γ-secretase with the D385-protonated PS1. (A) Residue-wise binding energy decomposition between γ-secretase and $C99_{\varepsilon 49}$ (black), $A\beta 49_{\zeta 46}$ (orange), $A\beta 46_{\gamma 43}$ (dark blue), $A\beta 43_{\gamma 40}$ (magenta), $A\beta 40_{\gamma 37}$ (green). Backbone (top) and sidechain (bottom) contributions are averaged through two replicas. **(B)** Residue-wise binding energy decomposition between γ-secretase and $A\beta 40_{\gamma 37}$ with wild-type (solid) G33I (brown), and K28A (yellow) mutated sequences. Backbone (top) and sidechain (bottom) contributions are averaged over two replicas. **(C)** Summation of substrate P5 and P6 sidechain binding energy contribution. The corresponding amino acids at P6 and P5 are annotated at the top of each bar.

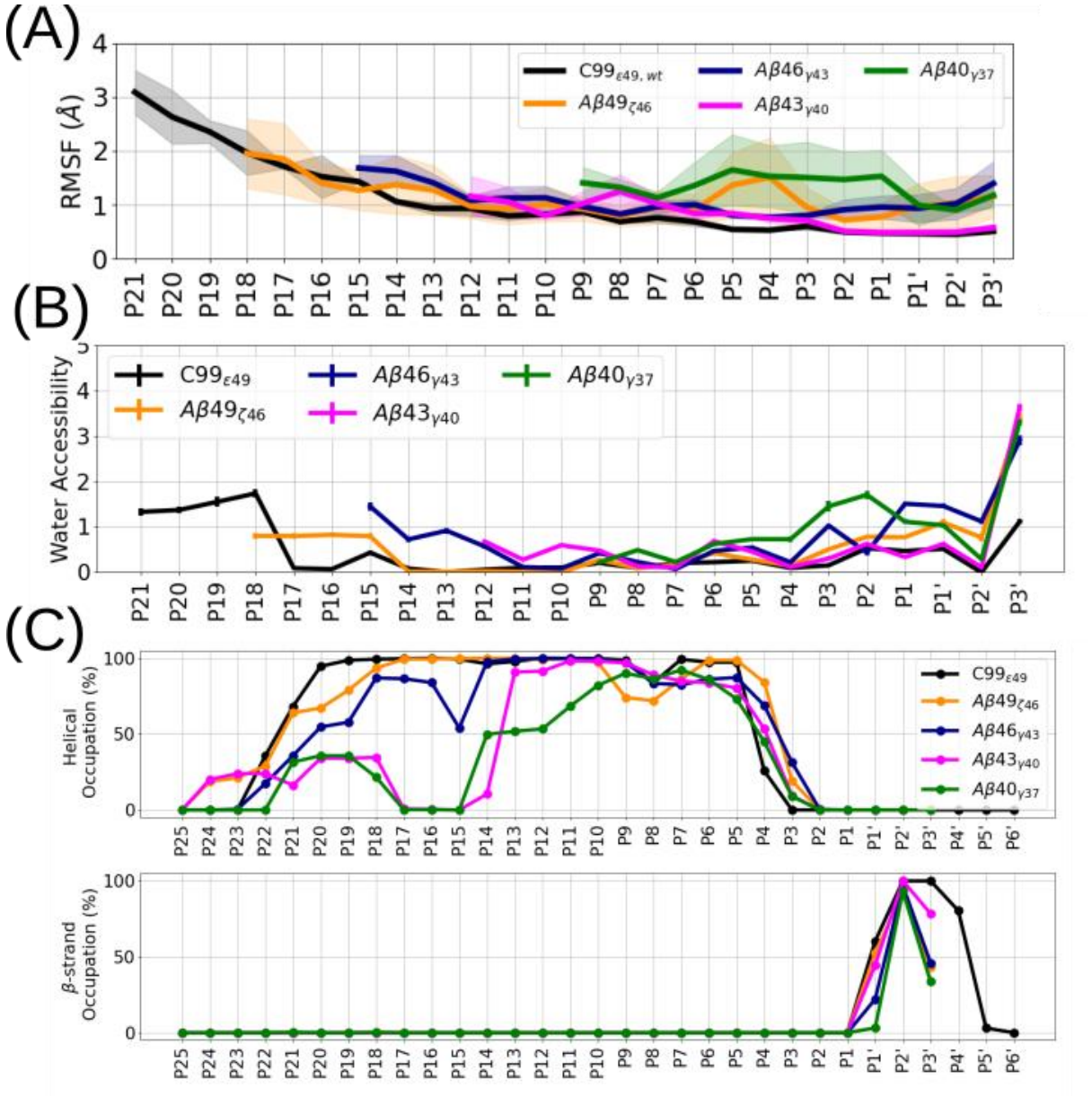

Figure S22: Properties of Aβ substrate bound with D385-protonated γ-secretase. (A) RMSF of the substrate TMD. **(B)** Residue-wise water accessibility. **(C)** Secondary structure analysis of C99 and Aβ peptides.

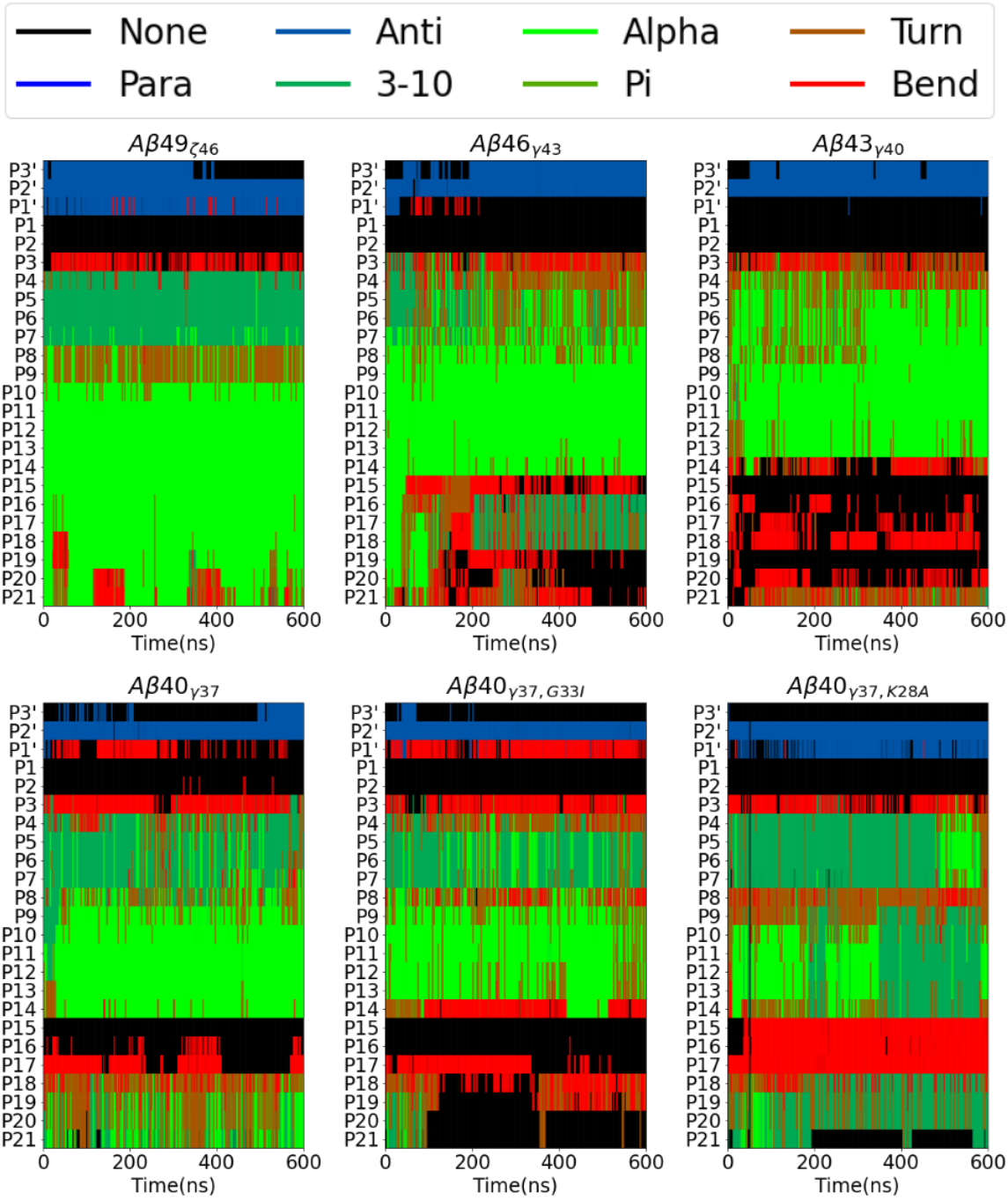

Figure S23: Evolution of secondary structure of the substrates in time. From left to right: (Top) Aβ49$_{\zeta 46}$, Aβ46$_{\gamma 43}$, Aβ43$_{\gamma 40}$, (Bottom) Aβ40$_{\gamma 37}$, Aβ40$_{\gamma 37,G33I}$, Aβ40$_{\gamma 37,K28A}$.

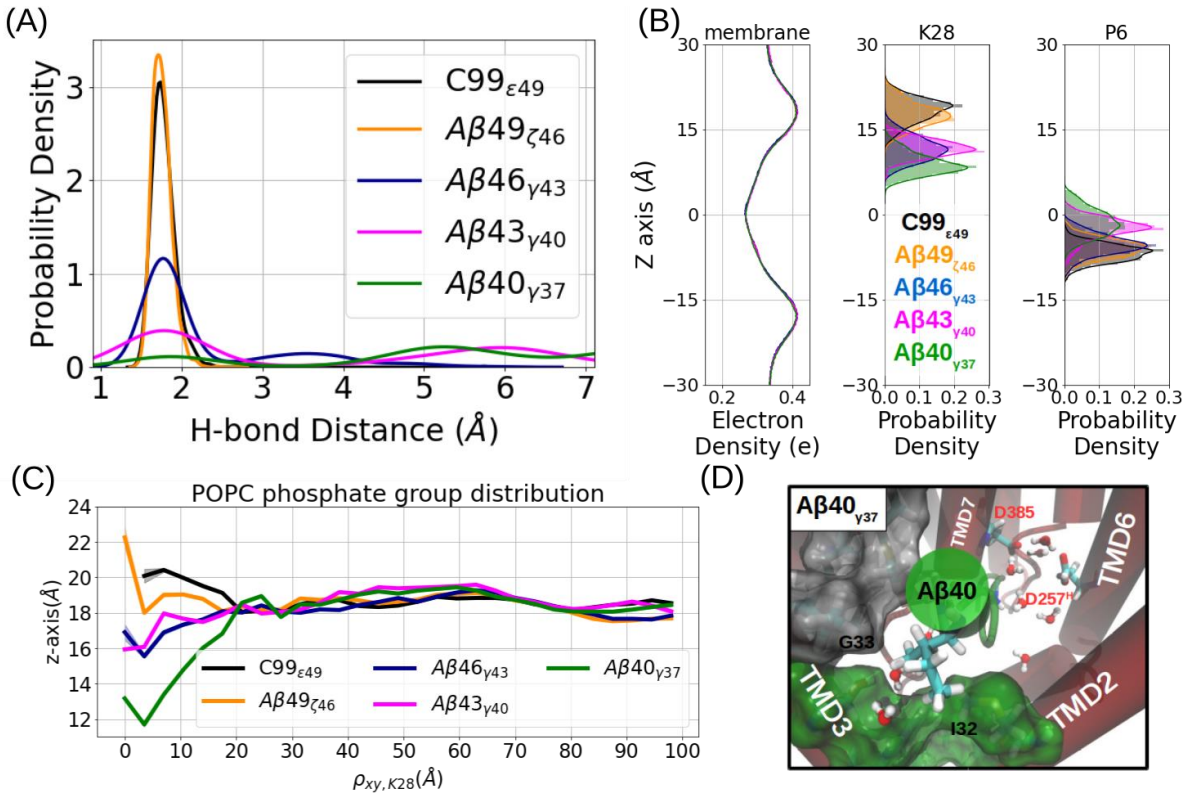

Figure S24: Comparative modeling and simulations of Aβn-γ-secretase complexes with D257-protonated PS1. (A) Probability density of the catalytic hydrogen bond distance. **(B)** Distribution of the calculated membrane electron/atom density (left), membrane-anchoring residue K28 (middle) and substrate P6 (right) along the z-axis in different Aβn-γ-secretase complexes. **(C)** Average z-axis of the POPC phosphate on the extracellular side distributed along the radial distance $\rho_{xy,K28}$. **(D)** View into the PS1 internal docking site in the Aβ40$_{\gamma37}$-bound γ-secretase. (representation same as in **Figure S6C**).

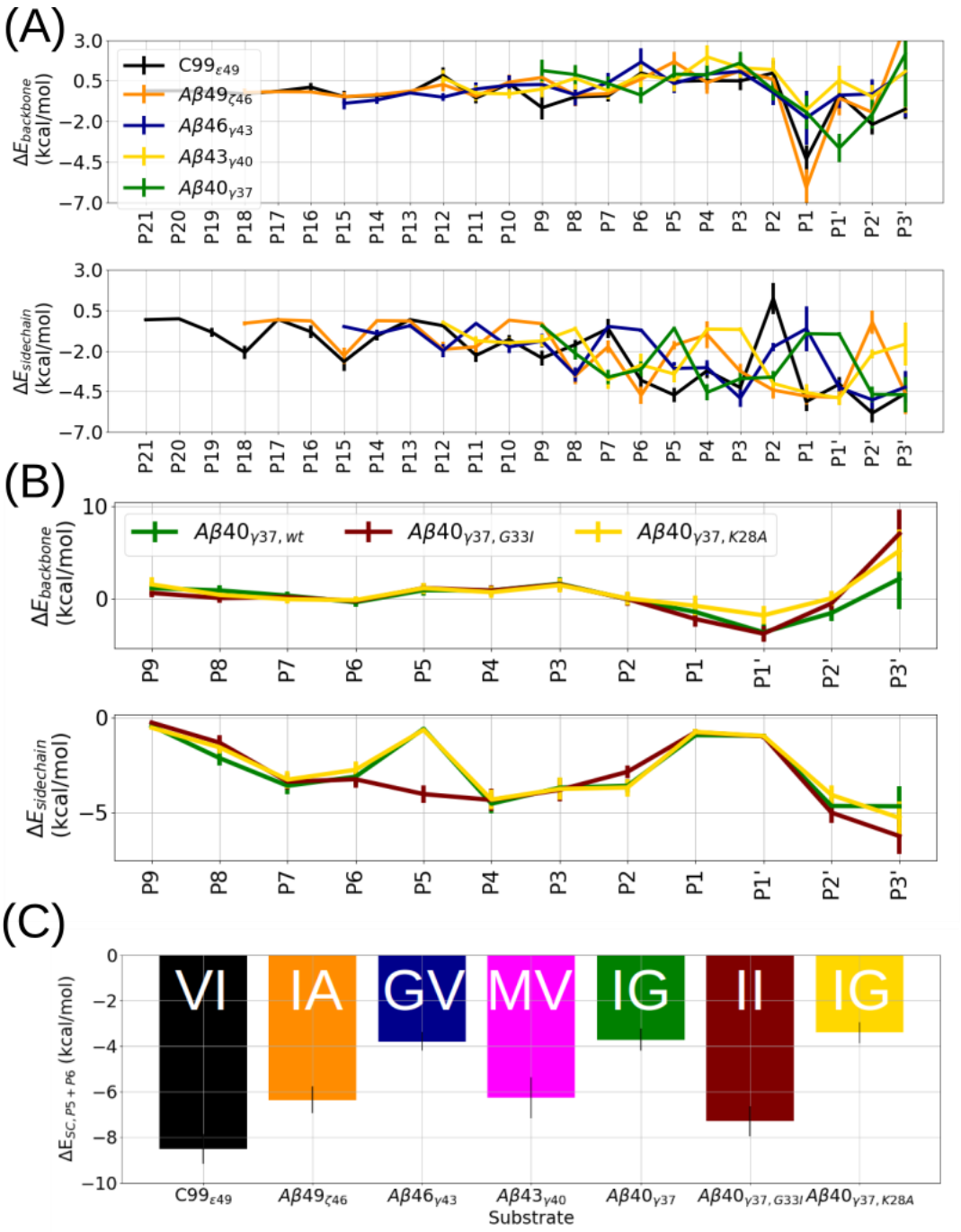

Figure S25: Binding energy between different substrates and γ-secretase with the D257-protonated PS1. (A) Residue-wise binding energy decomposition between γ-secretase and $C99_{\varepsilon 49}$ (black), $A\beta 49_{\zeta 46}$ (orange), $A\beta 46_{\gamma 43}$ (dark blue), $A\beta 43_{\gamma 40}$ (magenta), $A\beta 40_{\gamma 37}$ (green). Backbone (top) and sidechain (bottom) contributions are averaged through two replicas. **(B)** Residue-wise binding energy decomposition between γ-secretase and $A\beta 40_{\gamma 37}$ with wild-type (solid) G33I (brown), and K28A (yellow) mutated sequences. Backbone (top) and sidechain (bottom) contributions are averaged through two replicas. **(C)** Summation of substrate P5 and P6 sidechain binding energy contribution. The corresponding amino acids at P6 and P5 are annotated at top of each bar.

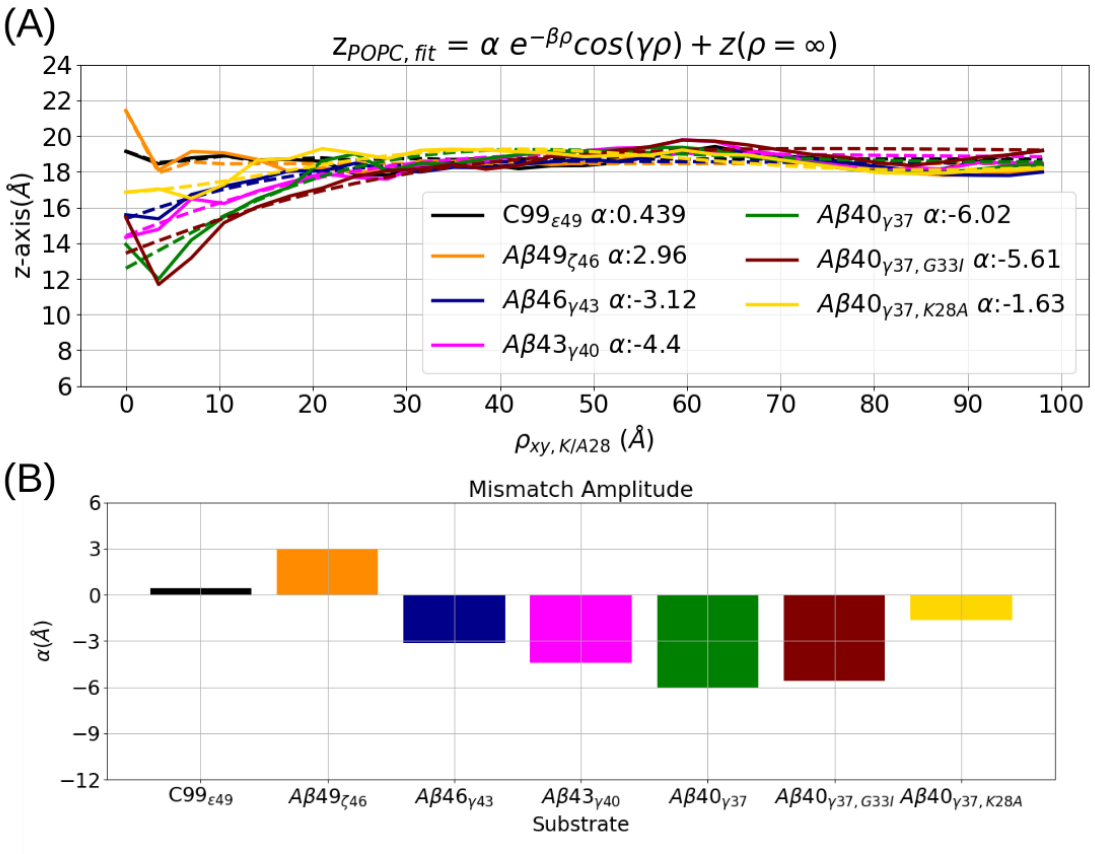

Figure S26: Fitting the membrane thickness distributed alone the radial distance on the xy plane from K/A28 of substrates with D257-protonated PS1. (A) Fitting the hydrophobic mismatch profile with hydrophobic mismatch amplitude α, radial decaying rate β, and harmonic oscillation γ. **(B)** Comparison of the hydrophobic mismatch amplitude α calculated from **(A)** in different Aβ-bound γ-secretase structures.

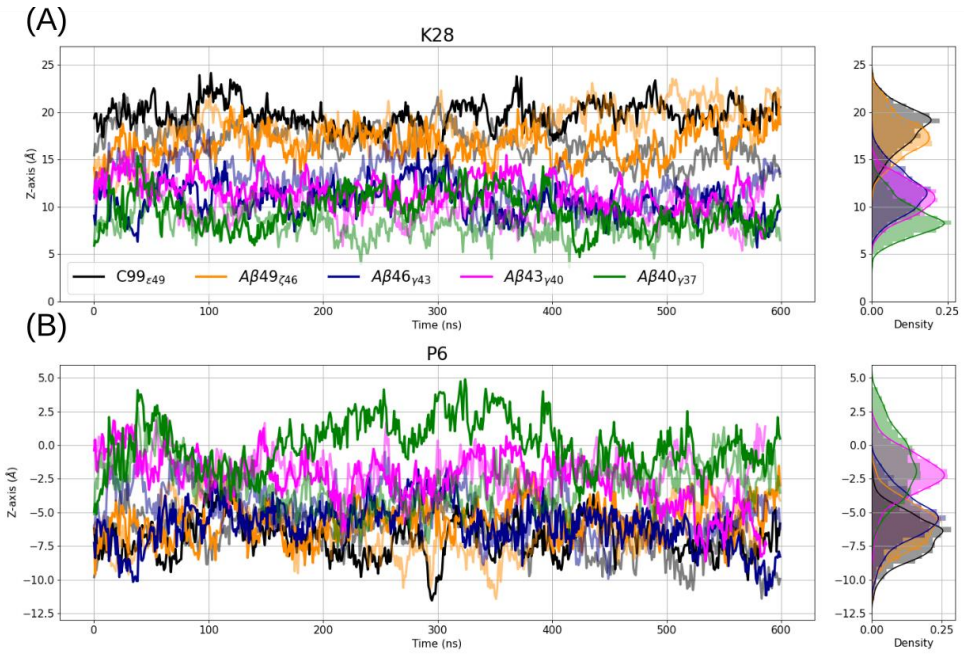

Figure S27: Z-axis position of substrate (A) K28 and (B) P6 in complex with γ-secretase with D257-protonated vs. simulation time. Two replicas are represented by solid and transparent lines in the same color. The averaged phosphate groups are located at z=18Å plane (see Figure S23C).

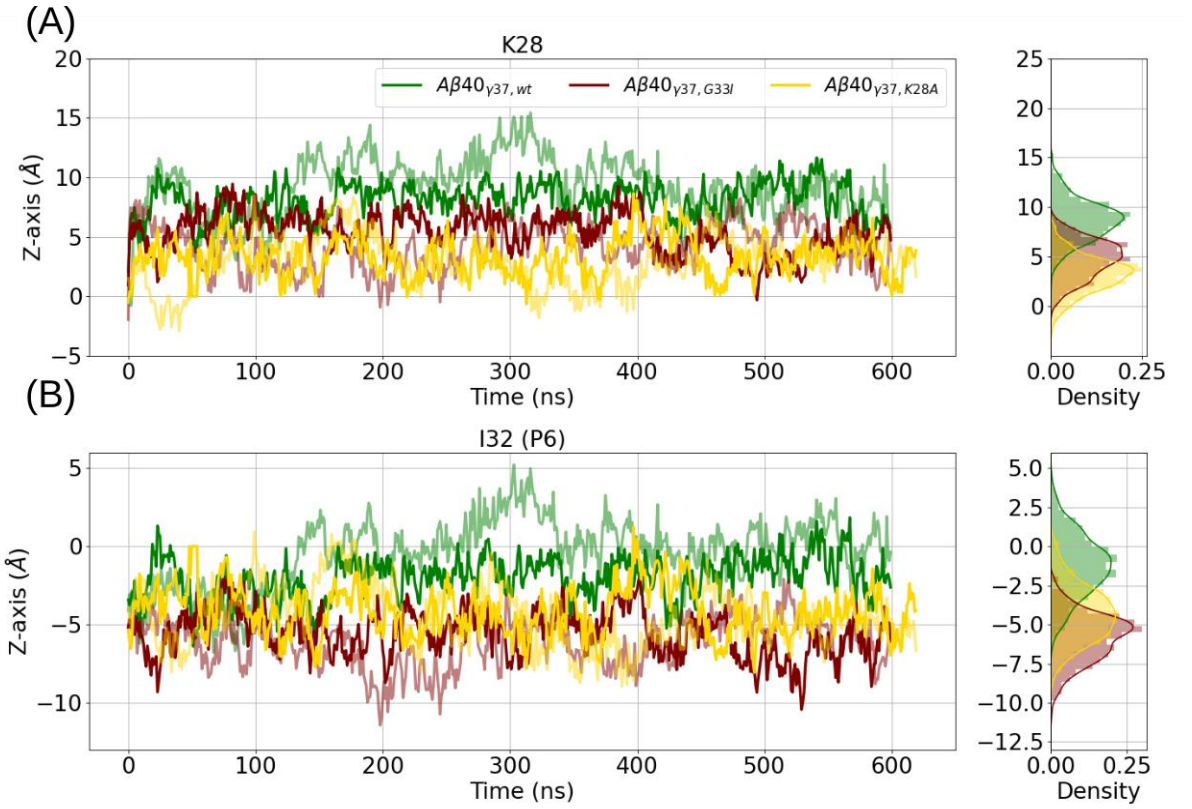

Figure S28: Z-axis position of substrate (A) K28 and (B) I32 in complex with γ-secretase with D385-protonated vs. simulation time. Two replicas are represented by solid and transparent lines in the same color. The averaged phosphate groups are located at z=18Å plane (see Figure 7C of the main text).

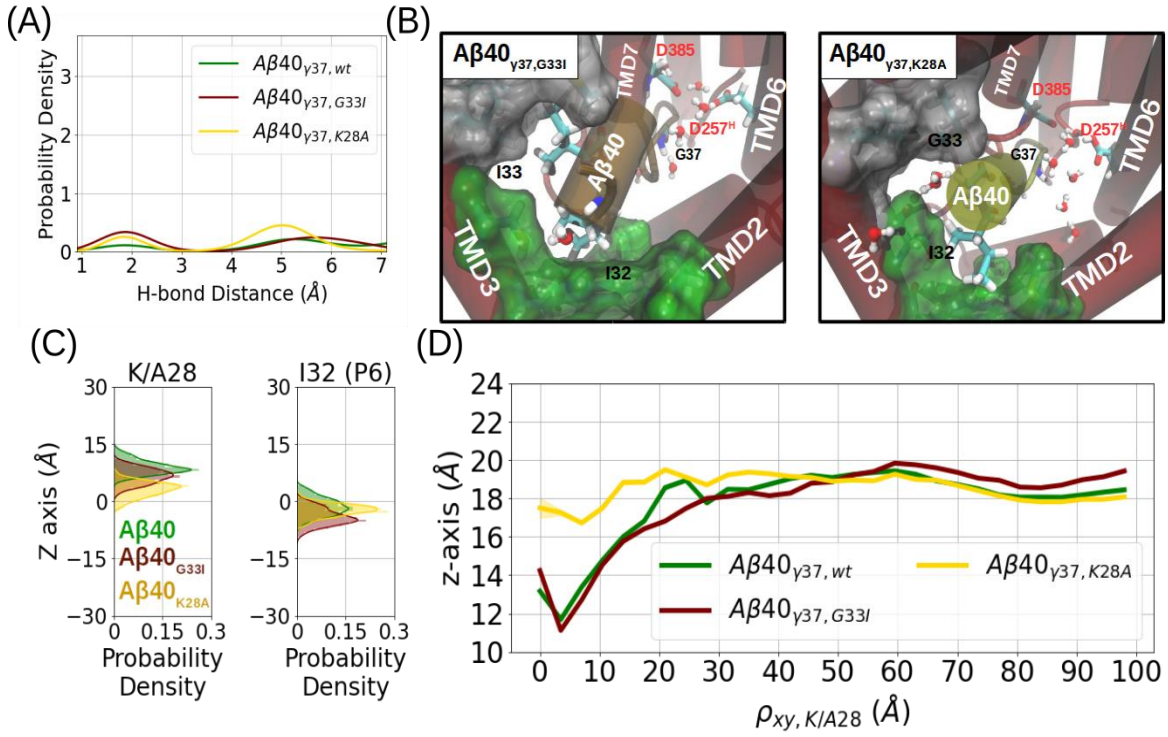

Figure S29: Influence of the APP mutations G33I and K28A on the Aβ40$_{γ37}$ binding pose with D257-protonated PS1. (A) Probability density of the catalytic hydrogen bond distance. **(C)** Distribution of the substrate K/A28 (middle) and substrate P6 (right) along the z-axis in different Aβn-γ-secretase complexes. **(D)** Average z-axis of the POPC phosphate on the extracellular side distributed along the radial distance $ρ_{xy,K28}$.

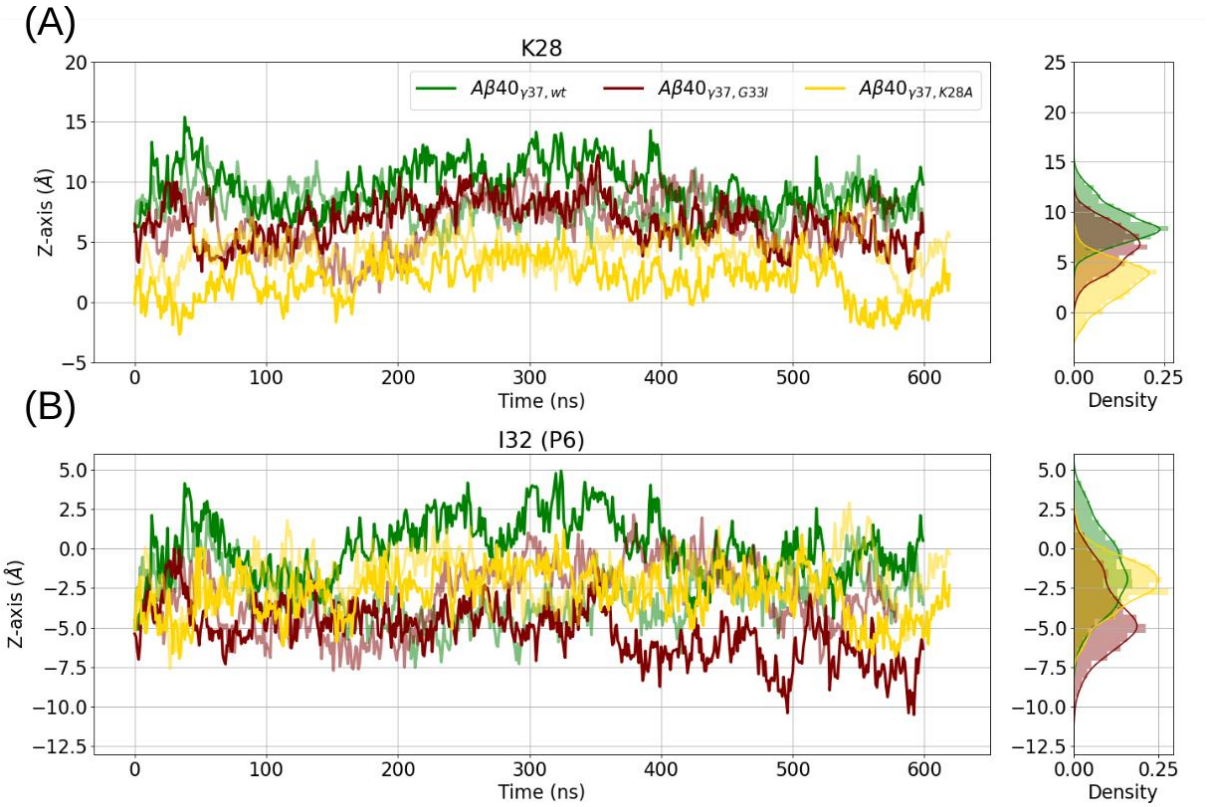

Figure S30: Z-axis position of substrate (A) K28 and (B) P6 in complex with γ-secretase with D257-protonated vs. simulation time. Two replicas are represented by solid and transparent lines in the same color. The averaged phosphate groups are located at z=18Å plane (see Figure S23C).

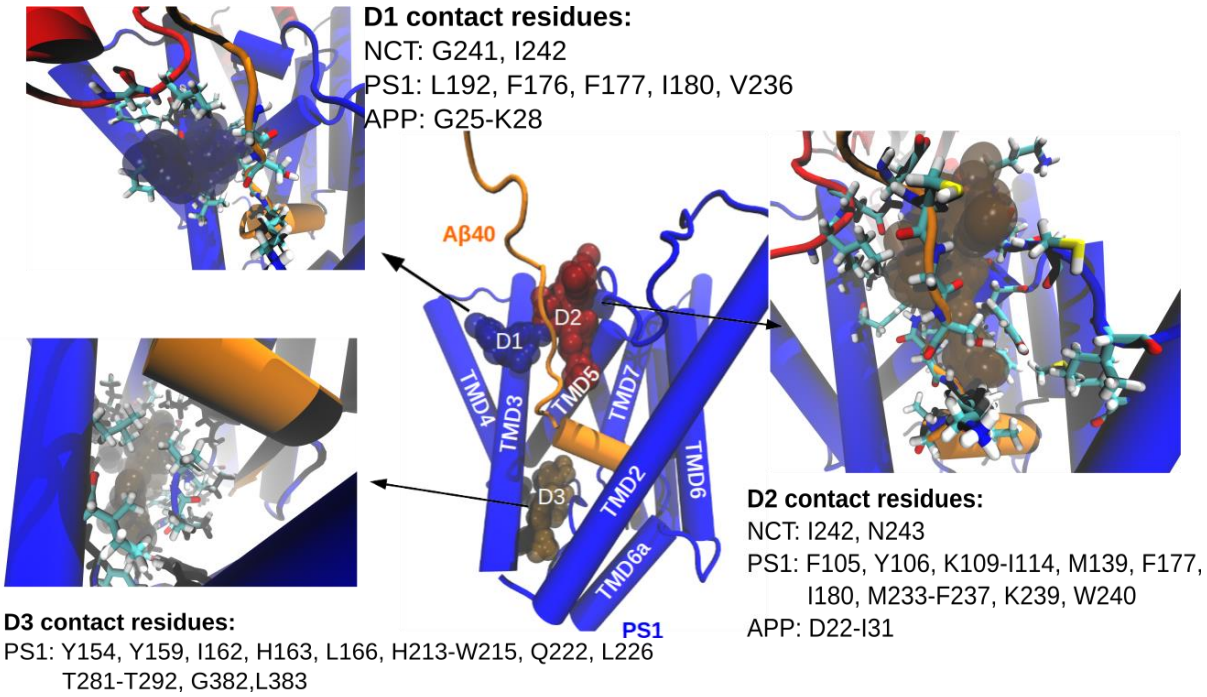

Figure S31: Probing of the potential ligand docking sites D1, D2, and D3 with Fpocket. Possible contacting residues in PS1 are indicated.